UV Resonance Raman and Circular Dichroism Studies of a DNA Duplex Containing an A_3T_3 Tract: Evidence for a Premelting Transition and Three-Centered H-Bonds†

Ishita Mukerji*,‡ and Alison P. Williams§,||

Department of Molecular Biology and Biochemistry, Molecular Biophysics Program, Wesleyan University, Middletown, Connecticut 06459, and Department of Chemistry, Rutgers University, Wright-Rieman Laboratories, 610 Taylor Road, Piscataway, New Jersey 08854

Received May 4, 2001

ABSTRACT: The presence of A_n and A_nT_n tracts in double-helical sequences perturbs the structural properties of DNA molecules, resulting in the formation of an alternate conformation to standard B-DNA known as B′-DNA. Evidence for a transition occurring prior to duplex melting in molecules containing A_n tracts was previously detected by circular dichroism (CD) and calorimetric studies. This premelting transition was attributed to a conformational change from B′- to B-DNA. Structural features of A_n and A_nT_n tracts revealed by X-ray crystallography include a large degree of propeller twisting of adenine bases, narrowed minor grooves, and the formation of three-centered H-bonds between dA and dT bases. We report UV resonance Raman (UVRR) and CD spectroscopic studies of two related DNA dodecamer duplexes, $d(CGCAAATTTGCG)_2$ (A_3T_3) and $d(CGCATATATGCG)_2$ [$(AT)_3$]. These studies address the presence of three-centered H-bonds in the B′ conformation and gauge the impact of these putative H-bonds on the structural and thermodynamic properties of the A_3T_3 duplex. UVRR and CD spectra reveal that the premelting transition is only observed for the A_3T_3 duplex, is primarily localized to the dA and dT bases, and is associated with base stacking interactions. Spectroscopic changes associated with the premelting transition are not readily detectable for the sugar−phosphate backbone or the cytosine and guanosine bases. The temperature-dependent concerted frequency shifts of dA exocyclic NH_2 and dT C4═O vibrational modes suggest that the A_3T_3 duplex forms three-centered hydrogen bonds at low temperatures, while the $(AT)_3$ duplex does not. The enthalpy of this H-bond, estimated from the thermally induced frequency shift of the dT C4═O vibrational mode, is approximately 1.9 kJ/mol or 0.46 kcal/mol.

DNA molecules containing oligo(dA)·oligo(dT) tracts have been shown to exhibit unusual physical properties, including reduced electrophoretic mobility compared to random sequences and fast overall rotational relaxation (for reviews, see refs *1* and *2*). These physical properties of the DNA were attributed to sequence-induced curvature, caused by the presence of the oligo(dA)·oligo(dT) tracts. Maximal bending occurs when the tracts are approximately half the length of a helical turn and are repeated in phase with the DNA helix (*1*). These types of sequences first observed in kinetoplast DNA have subsequently been observed at the origin of replication of prokaryotic and eukaryotic DNA, suggesting that sequence-induced curvature of DNA may play a functional role in biological processes (*3*).

X-ray crystallographic characterization of relatively short DNA duplexes containing A tracts has shown that the A tract region has a narrowed minor groove and is relatively straight and rigid (*4*−*6*). The large propeller twisting observed for the adenine residues within the A tracts themselves accounts in part for the observed rigidity (*7*). The X-ray crystal structures of oligo(dA)·oligo(dT) and A_nT_n tracts reveal that this propeller twisting of the adenine residues may be stabilized by the formation of a cross-strand three-centered H-bond between the exocyclic N6 amino group of the adenosine and the C4 carbonyl group of the thymidine residues (Figure 1) (*4*, *6*, *8*). NMR characterization of a DNA duplex containing an A_3T_3[1] tract detected elevated activation enthalpies and entropies of amino group rotation for the central A5 residue, consistent with the formation of a three-centered H-bond (*9*). More recently, an NMR structural determination of an A tract-containing sequence has also yielded interstrand distances indicative of bifurcated H-bond formation (*10*).

The level of DNA curvature associated with A_n and A_nT_n tracts is markedly reduced at higher temperatures, as shown

† This work was supported by a National Science Foundation Career Development Award (MCB-9507241) and a grant from the Patrick and Catherine Weldon Donaghue Medical Research Foundation (DF96-175). A.P.W. gratefully acknowledges support from NIH Grant GM 37909 (awarded to David L. Beveridge, Wesleyan University) and Grant GM 48802-06 (awarded to Roger A. Jones, Rutgers University).

* To whom correspondence should be addressed. Phone: (860) 685-2422. Fax: (860) 685-2141. E-mail: imukerji@wesleyan.edu.

‡ Wesleyan University.

§ Rutgers University.

|| Present address: Department of Chemistry, Frick Chemical Laboratories, Princeton University, Princeton, NJ 08544.

[1] Abbreviations: UVRR, ultraviolet resonance Raman; CD, circular dichroism; A_3T_3, 5′-CGCAAATTTGCG-3′; $(AT)_3$, 5′-CGCATATATGCG-3′; MWCO, molecular weight cutoff; EDTA, *N*,*N*,*N*′,*N*′-ethylenediaminetetraacetic acid; T_m, melting temperature.

10.1021/bi010918i CCC: $22.00
Published on Web 12/07/2001

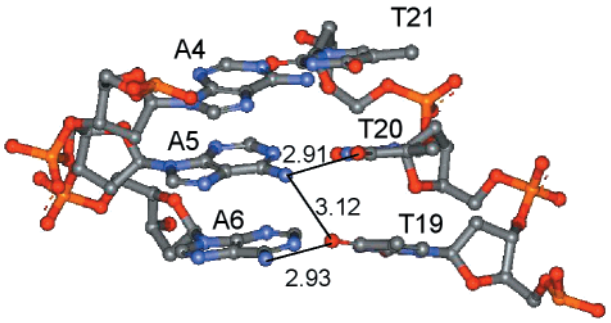

FIGURE 1: Schematic representation of the A tract region of the A_3T_3 dodecamer duplex depicting the three-centered H-bond among A5, T20, and T19. The Watson−Crick H-bond between A6 and T19 is also shown. This diagram was made using Weblab Viewer Lite and the X-ray crystallographic coordinates of Edwards et al. (*6*) (NDB entry BDL038).

by a reduction in the degree of anomalous gel migration behavior. Other evidence for a reduced level of curvature is obtained from electron microscopy, NMR, and rotational dynamic studies, which were also suggestive of a conformational change with an increase in temperature prior to the conversion to single strands (*11*). Energetically, a DNA decamer containing an A_4T_4 tract (*12*) and longer DNA molecules containing homo dA·dT regions (*13*, *14*) exhibited broad premelting transitions, centered at 35 °C. These transitions were primarily observed by differential scanning calorimetry and CD spectroscopy (*12*, *14*). The premelting transition is distinct from the global melting of the duplex and was attributed to the conversion of the DNA molecules from a B′ or bent form of DNA to B-form DNA.

More recently, the premelting state of poly(dA)·poly(dT) has been characterized by UV resonance Raman spectroscopy (UVRR) (*15*). In this study, melting of the homopolymer as monitored by UVRR was compared with that of the alternating copolymer poly(dA-dT)·poly(dA-dT), which is not expected to form three-centered H-bonds because of the alternating sequence of adenosine and thymidine residues. This study revealed that the thymidine C4═O vibrational modes of the homopolymer shift in frequency over the temperature range of the premelting transition. This frequency shift was indicative of an increase in the force constant or bond order of the C4 carbonyl group, consistent with a decrease in H-bond strength. Comparable frequency shifts were not detected with the alternating copolymer, suggesting that the low-temperature structure of poly(dA)·poly(dT) contains propeller-twisted adenosine residues that form three-centered H-bonds (*15*). Furthermore, the observation of this feature at low temperatures and the disappearance at higher temperatures is suggestive of a correlation with DNA bending (*1*).

In the investigation described here, we have examined these structural and energetic features in two DNA dodecamers, which have been characterized by X-ray crystallography (*5*, *6*, *16*). These dodecamers, 5′-CGCAAATTTGCG-3′ and 5′-CGCATATATGCG-3′ [hereafter termed A_3T_3 and $(AT)_3$, respectively], have the same base composition and, at the 5′ and 3′ ends, the same base sequence. Most significant is the fact that in the central 6 bp region the A_3T_3 dodecamer contains an A_nT_n tract while the $(AT)_3$ dodecamer contains alternating A-T residues. Using UV resonance Raman and circular dichroism spectroscopic methods, we have characterized the premelting and melting transitions of these two DNA duplexes.

A tract-dependent curvature has been described as a cooperative phenomenon, which is dependent on DNA length (*17*). In this study, we examine the structure and energetics of a sequence which contains only one short A_3T_3 tract, which is not expected to exhibit significant cooperativity. The results are compared with those obtained previously on a longer A tract (*15*). The UVRR and CD results reveal a premelting transition centered at 35 °C for the A tract-containing duplex. The temperature-dependent frequency shifts of the dT carbonyl and dA amino functional groups detected by UVRR and previously observed for the homopolymeric (dA)·(dT) species are observed in the A_3T_3 dodecamer, suggesting that the molecular basis of the B′-DNA structure is comparable in short and long A tracts. In addition, by comparing such well-defined molecular systems, we have been able to quantitatively characterize the relative strength of the putative three-centered H-bond and assess its energetic contribution to the premelting transition and stabilization of A_nT_n tracts.

MATERIALS AND METHODS

Purification of Oligonucleotides. Oligonucleotides were synthesized in 1 μmol quantities (Integrated DNA Technologies). Tritylated oligomers were purified as previously described (*18*). Deblocked and desalted oligomers were purified by polyacrylamide gel electrophoresis (*19*). Oligonucleotides were purified to >98% purity as judged by analytical gel electrophoresis. Prior to the spectroscopic experiments, the oligonucleotides were dialyzed extensively against the desired buffer in a Spectra-por microdialyzer with a 1000 MWCO membrane. To prepare duplexes, samples were heated at 95 °C in a water bath for 5 min and cooled slowly to room temperature. Once samples were cooled to 5 °C, they were maintained at that temperature through all manipulations until the melting experiments were performed.

Circular Dichroism. For circular dichroism (CD) measurements, samples were dialyzed against a 1.0 M Na^+ buffer containing 10 mM sodium cacodylate and 10 μM Na_2EDTA (pH 7.0). The Na_2EDTA concentration was decreased to minimize the absorbance below 220 nm. CD spectra were measured on an AVIV model 62A DS spectrometer with a Peltier temperature controller. Spectral scans were measured from 320 to 210 nm with a bandwidth of 1.0 nm and a 5 s averaging time. Samples were equilibrated at 0 °C for 15 min. The equilibration time for subsequent temperatures was 2 min. CD melts were measured at five distinct wavelengths. These melts were performed using a 0.5 °C step and a 1 min equilibration time. The averaging time was 10 s. To account for differences in concentration, CD spectra measured in millidegrees were converted to molar ellipticity ($\Delta\epsilon = \epsilon_L - \epsilon_R$) in units of inverse molar per centimeter. CD spectra taken before and after the melting process were essentially identical, indicating a reversible process.

Ultraviolet Resonance Raman Spectroscopy. The UV resonance Raman spectrometer has been previously described (*18*, *20*). Oligonucleotides were examined at a concentration of $1.0-1.25 \times 10^{-4}$ M in a solution containing 10 mM sodium cacodylate (pH 7.0) and 0.3 M Na_2SO_4. The Na_2SO_4 acts as an internal frequency and intensity standard.

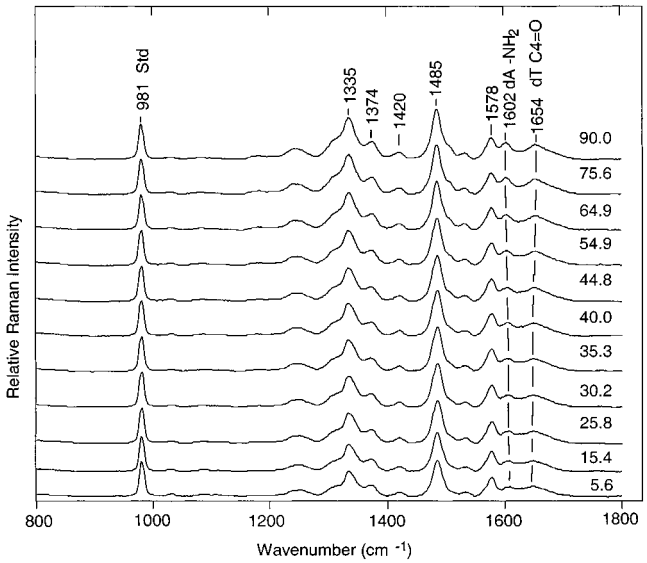

FIGURE 2: UV resonance Raman spectra of the A_3T_3 duplex obtained with 260 nm excitation. Spectra were obtained at the indicated temperatures and normalized to the intensity standard Na_2SO_4 at 981 cm^{-1}. The DNA concentration was 1.46×10^{-4} M in a 10 mM cacodylate buffer (pH 7.0) containing 0.3 M Na_2SO_4.

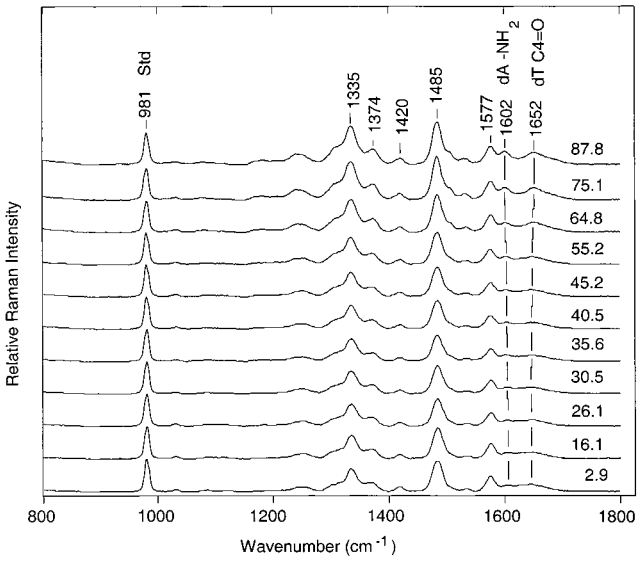

FIGURE 3: UV resonance Raman spectra of the $(AT)_3$ duplex obtained with 260 nm excitation. Spectra were obtained at the indicated temperatures and normalized to the intensity standard Na_2SO_4 at 981 cm^{-1}. The DNA concentration was 1.35×10^{-4} M in a 10 mM cacodylate buffer (pH 7.0) containing 0.3 M Na_2SO_4.

Samples were contained in a cylindrical quartz cuvette with a diameter of 0.3 cm (NSG Precision Cells) and were stirred continuously. The temperature at the sample was maintained with an aluminum block cell holder and a circulating bath and was monitored with a Cu-constantan thermocouple at the block. Each spectrum results from 0.5 h of data collection acquired in three cycles of 10 min each. Samples were characterized by UV−vis absorption spectroscopy and analytical gel electrophoresis before and after UVRR spectroscopy; no evidence of degradation was observed.

RESULTS

The 260 nm-Excited UVRR Spectra. (1) Intensity Changes. Using an excitation wavelength of 260 nm, the melting of the A_3T_3 (Figure 2) and $(AT)_3$ (Figure 3) duplexes has been monitored using UVRR spectroscopy. At this excitation wavelength, dA and dT residues contribute most strongly to the observed spectrum (*21*). As the temperature is increased from 5 to 90 °C, the intensity of all the UVRR modes increases substantially as measured relative to the internal intensity standard, Na_2SO_4 at 981 cm^{-1}. Base stacking interactions, which give rise to absorption hypochromism, also lead to the suppression of resonance Raman intensities because the intensities are proportional to the electronic absorption at the excitation wavelength. The two most intense modes in the 260 nm-excited spectra occur at 1335 and 1485 cm^{-1} and experience the greatest change in intensity with increasing temperatures. As a function of thermal denaturation, the 1485 cm^{-1} mode for both duplexes experiences an intensity increase of 34%. This comparable change in intensity suggests that the overall reduction in the extent of base stacking interactions is similar for the two duplexes.

Melting profiles generated from the mode intensities (Figure 4) reveal, however, that the melting process is distinctly different for the two duplexes. Specifically, the A_3T_3 duplex experiences a significant increase in Raman mode intensity before the expected duplex melting temperature (T_m) such that approximately 50% of the total intensity change has occurred by 40 °C. In contrast, the $(AT)_3$ duplex does not experience a significant change in Raman mode intensity until approximately 60 °C, which corresponds to the T_m determined by UV absorption spectroscopy (Table 1).

Table 1: Duplex Melting Temperatures (°C) of A_3T_3 and $(AT)_3$

DNA duplex	A260[a]	ϵ255[b]	ϵ265[b,c]	ϵ285[b,c]	I1485[d]	calcd[e]
A_3T_3	67	66	66	68	65	68
$(AT)_3$	63	68	−	−	60	63

[a] Determined from temperature-dependent UV absorbance measurements. [b] Determined from temperature-dependent CD measurements. [c] The relatively shallow melting profile of the $(AT)_3$ duplex precludes determination of a T_m by a first derivative at 265 and 285 nm. [d] T_m determined from temperature-dependent UVRR measurements (Figure 4b). [e] T_m calculated from the nearest neighbor thermodynamic parameters of Santa-Lucia et al. (*27*) at a DNA concentration of 0.1 mM.

The modes shown in Figure 4 arise from ring stretching and bending motions of the dA and dT residues. Specifically, the 1485 cm^{-1} mode arises from bending motions of the C2−H and C8−H bonds coupled with stretching of the C8−C9 bond, and the 1335 cm^{-1} mode mainly arises from stretching vibrations of the imidazole ring (*21*, *22*). The 1604 and 1650 cm^{-1} modes correspond to dA NH_2 scissors and dT C4═O stretching vibrations, respectively. All of these vibrations are coupled to stretching vibrations of their respective rings, leading to their resonance enhancement (*21*−*23*). Other vibrational modes arising from adenosine and thymidine yield comparable melting profiles for both duplexes (data not shown). The pronounced increase in the Raman intensity of the A_3T_3 duplex, centered at approximately 35 °C, is attributed to a premelting transition of the A_3T_3 tract (*11*−*14*).

(2) Frequency Changes. Similar temperature-dependent changes are observed for the frequency of the dT C4═O stretching vibration occurring at 1645 cm^{-1} at 5 °C (Figure 5a). This mode is comprised of both C4═O and C5═C6 stretching vibrations (*23*) and is sensitive to H-bonding at

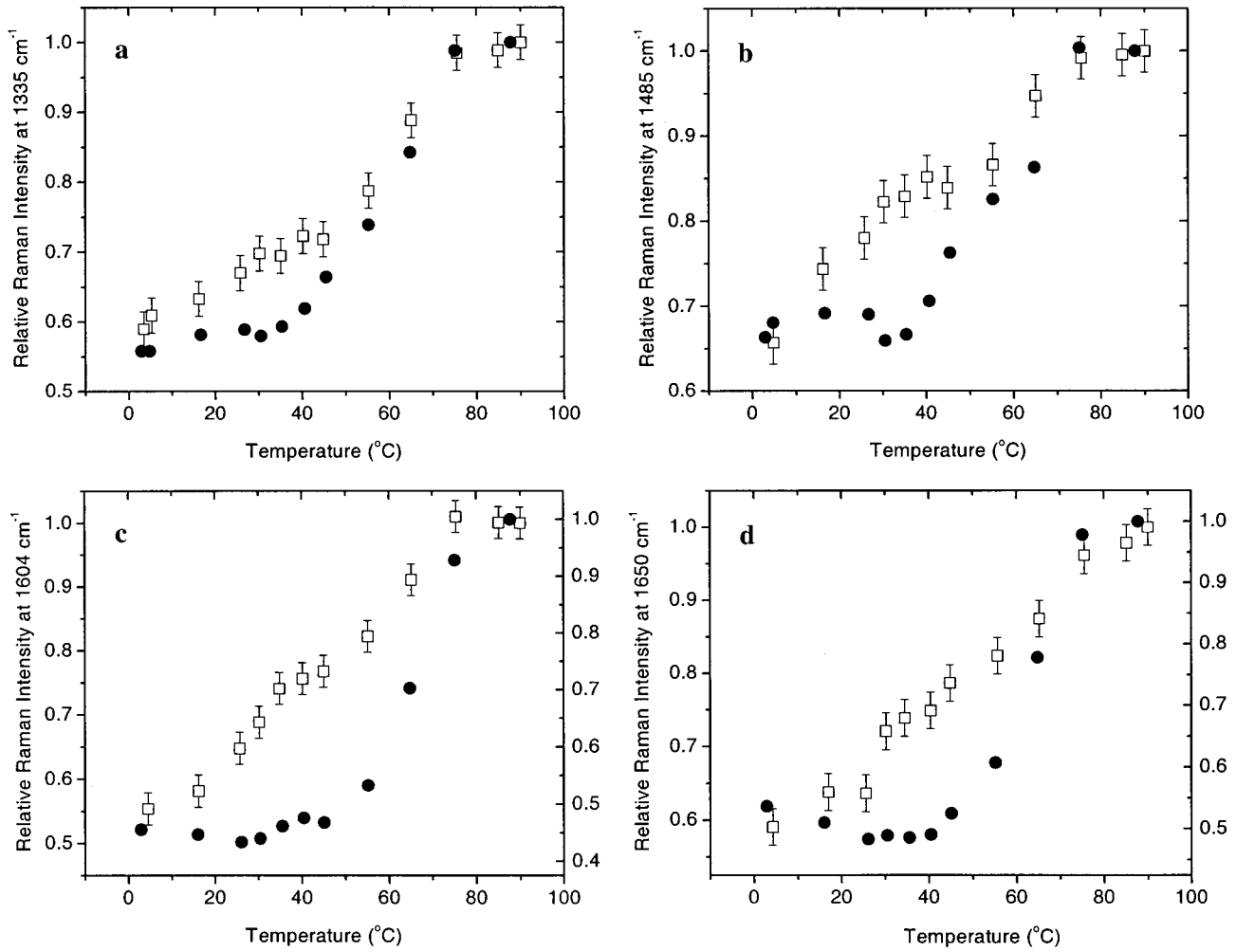

FIGURE 4: (a−d) Temperature-dependent relative UV Raman intensities of the 1335, 1485, 1604, and 1650 cm^{-1} modes of the A_3T_3 (□) and $(AT)_3$ (●) duplexes obtained with 260 nm excitation. All intensities that are shown represent an average of at least two different data sets and have been normalized to their maximum value. Sample conditions were as described in the legends of Figures 2 and 3. For clarity, error bars are shown for the A_3T_3 data only, and comparable error bars can be drawn for the $(AT)_3$ data. In panels c and d, the A_3T_3 data are shown with the left axis and $(AT)_3$ data with the right axis.

the C4 carbonyl group (*15*, *24*). Carbonyl stretching vibrations typically experience an increase in vibrational frequency with a reduction in H-bonding strength (*20*). For 1-methylthymine, comparable frequency shifts of the C4═O stretching vibration were observed in a non-H-bond-donating solvent compared to water (*24*). In the case of the A_3T_3 duplex, a significant portion of the frequency shift occurs before the duplex melting temperature (∼65 °C) has been reached. Thus, the increase in the C4═O stretching frequency of the A_3T_3 duplex occurs concurrently with the observed changes in Raman intensity and at a lower temperature than the $(AT)_3$ duplex.

The changes in the dT C4═O stretching frequency are also correlated with a frequency shift of the dA NH_2 scissors vibration in the A_3T_3 duplex, as shown in Figure 5b. The scissors vibration which is coupled to a ring vibration of the adenosine pyrimidine ring shifts to lower frequency with a weakening of H-bonding at the NH_2 functional group (*15*, *23*, *24*). Thus, the increase in the dT C4═O stretching frequency (from 1645 to 1655 cm^{-1}) and the decrease in the dA NH_2 scissors frequency (from 1608 to 1602 cm^{-1}) are both consistent with a reduction in H-bonding strength with an increase in temperature. The correlated nature of the frequency changes strongly suggests that they arise from a reduction in H-bond strength between these two functional groups. For the dT C4═O (Figure 5a) and the dA NH_2 vibrations, the magnitude of the frequency change as a function of temperature for the A_3T_3 duplex is larger than that obtained for the $(AT)_3$ duplex. At temperatures <55 °C, the changes in frequency of these two groups are attributed to a reduction in the strength of a cross-strand three-centered H-bond between A5 and T19 as observed in the X-ray crystal structure (Figure 1) (*6*). Similar frequency changes were observed in an UVRR investigation of poly(dA)·poly(dT) and were ascribed to a loss in strength of a three-centered H-bond during the premelting transition (*15*).

Circular Dichroism Spectra. The melting behavior of the two dodecamer duplexes was also examined by CD spectroscopy (Figure 6). The temperature-dependent spectra of both duplexes reveal spectral features at low temperatures that are indicative of general B-DNA structure (*25*). Specifically, the A_3T_3 duplex exhibits maxima at 284.5 and 219 nm and a minimum centered at 253 nm, and the $(AT)_3$ duplex exhibits maxima at 279 and 226 nm and a minimum at 251 nm. At shorter wavelengths (<230 nm), the spectrum of the $(AT)_3$ dodecamer is similar to that obtained for poly(dA-dT)·poly(dA-dT) (*26*). At higher temperatures, the spectra of the two duplexes closely resemble each other, as expected.

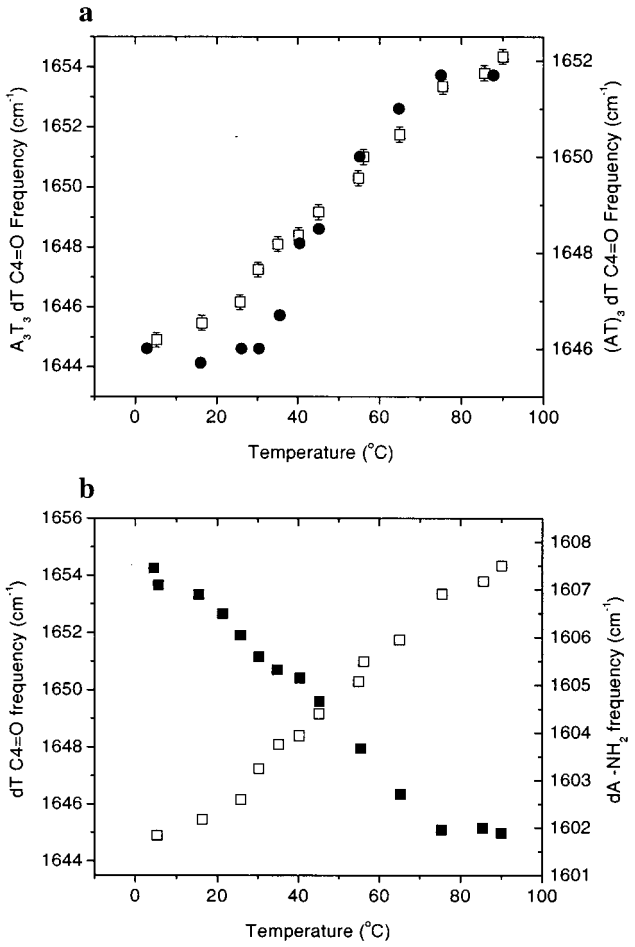

FIGURE 5: (a) Temperature-dependent UVRR frequency of the dT C4═O mode of the A_3T_3 (□, left axis) and $(AT)_3$ (●, right axis) duplexes obtained with 260 nm excitation. Frequencies result from an average of at least two different data sets. (b) Comparison of the temperature-dependent UVRR frequencies of the dT C4═O (□, left axis) and dA NH_2 (■, right axis) modes for the A_3T_3 duplex. Frequencies result from an average of at least two different data sets. For clarity, representative error bars for all data sets are shown for the A_3T_3 data in panel a.

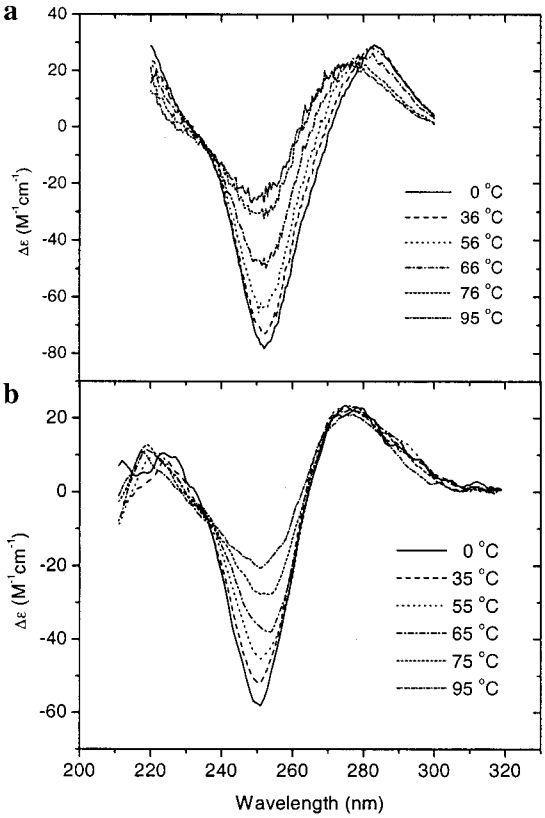

FIGURE 6: Temperature-dependent CD spectra. (a) A_3T_3 duplex, where the concentration was 1.48×10^{-4} M in 10 mM cacodylate buffer (pH 7.0) with 1.0 M Na^+ and 10 μM Na_2EDTA. (b) $(AT)_3$ duplex, where the concentration was 2.18×10^{-5} M in 10 mM cacodylate buffer (pH 7.0) with 1.0 M Na^+ and 10 μM Na_2EDTA. Measurements were taken at the indicated temperatures.

For the A_3T_3 duplex, the largest change in CD intensity is observed at 255 nm; a smaller intensity change coupled with a peak wavelength shift (283 → 278 nm) occurs at wavelengths above 275 nm. Interestingly, the $(AT)_3$ duplex, which also has a large temperature-dependent intensity change at 250 nm, exhibits minimal intensity changes above 275 nm and no change in peak wavelength.

A comparison of the molar ellipticity at 255 nm as a function of temperature (Figure 7a) demonstrates that the A_3T_3 duplex begins melting at a lower temperatures than does the $(AT)_3$ duplex. This behavior, as in the UVRR data, is suggestive of a premelting transition in the A_3T_3 duplex that is not present in the $(AT)_3$ duplex. This premelting transition appears to be centered between 30 and 35 °C (Table 2). In an earlier report, Chan and co-workers proposed that the ellipticity at 247 nm mainly monitored the global duplex to single-strand transition and the ellipticity at 285 nm monitored a unimolecular premelting transition between B′- and B-DNA (*13*). These measurements were taken with poly(dA)·poly(dT) and kinetoplast DNA. We observe that the temperature dependence of the CD data is highly wavelength-dependent, and a comparison of melting data obtained at 250 nm provides little evidence for a premelting transition, in agreement with the findings of Chan and co-workers (*13*). In contrast, melting data obtained for the A_3T_3 duplex at 260 (data not shown) and 265 nm (Figure 7b) reveal significant increases in molar ellipticity at temperatures consistent with a premelting transition.

In the CD data, the convolution of the premelting and global duplex melting transitions leads to an apparent lower T_m for the A_3T_3 duplex at 255 nm (Figure 7a). This finding is in contrast to the predicted melting behavior of these duplexes based on empirically derived thermodynamic parameters (*27*) (Table 1). Interestingly, the CD-determined T_m of the $(AT)_3$ duplex is higher than that determined by UV absorption or UV resonance Raman spectroscopic methods (Table 1). At this time, the origin of the elevated T_m of the $(AT)_3$ duplex as measured by CD is not known. At wavelengths which yield a better separation of the premelting and duplex transitions or wavelengths that are solely reflective of the duplex transition, the T_ms determined for the A_3T_3 duplex are more consistent with the expected values (Table 1).

We find, however, that the molar ellipticity at 285 nm does not show any evidence of a premelting transition (Figure 7b). Ellipticity changes above 275 nm have been correlated with the degree of twisting of the duplex (*28*). It is possible that the longer A tracts and homopolymer used in the earlier studies (*13*, *14*) experienced a greater degree of untwisting during the premelting transition than the relatively short dodecamer duplexes used in the study presented here. We

Table 2: Enthalpic Contribution of the Premelting Transition

DNA duplex	T_m (°C)	ΔH [kcal (mol·cu)$^{-1}$]	ΔH [kcal (mol·bp)$^{-1}$]	ΔH [kcal (mol·A·T bp)$^{-1}$]	ΔH [kcal (mol·A·A steps)$^{-1}$]	percent relative contribution of the three-centered H-bond[a]
poly(dA)·poly(dT)[b]	34.5	20.2[c]	1.8			
$[d(GA_4T_4C)]_2$[d]	28	16.0	1.6	2.0	2.2	
phased (A_5)[e]	32	70[f]	1.6	3.5	4.4	
A_3T_3[g]	30	15.1	1.3	2.5	3.8	13

[a] The percent relative contribution is defined as the ΔH of the three-centered H-bond determined from UVRR measurements relative to the ΔH (kilocalories per mole per A-A step) determined from CD measurements multiplied by 100. [b] The reported values represent averages of two independent studies using temperature-dependent CD (*13*) and UV absorbance (*30*) measurements. [c] The cooperative unit of poly(dA)·poly(dT) has been calculated to be 11 bp (*11*). [d] The reported values are from a calorimetric determination of the premelting transition (*12*). [e] Reported values were determined by differential scanning calorimetry of a 45 bp duplex containing four phased $(dA)_5$ tracts (*14*). [f] This value was determined for the 45 bp duplex; in the same study (*14*), temperature-dependent CD measurements yielded a value of 16 kcal/mol per cu. [g] Reported values are derived from the temperature-dependent CD measurements of this work.

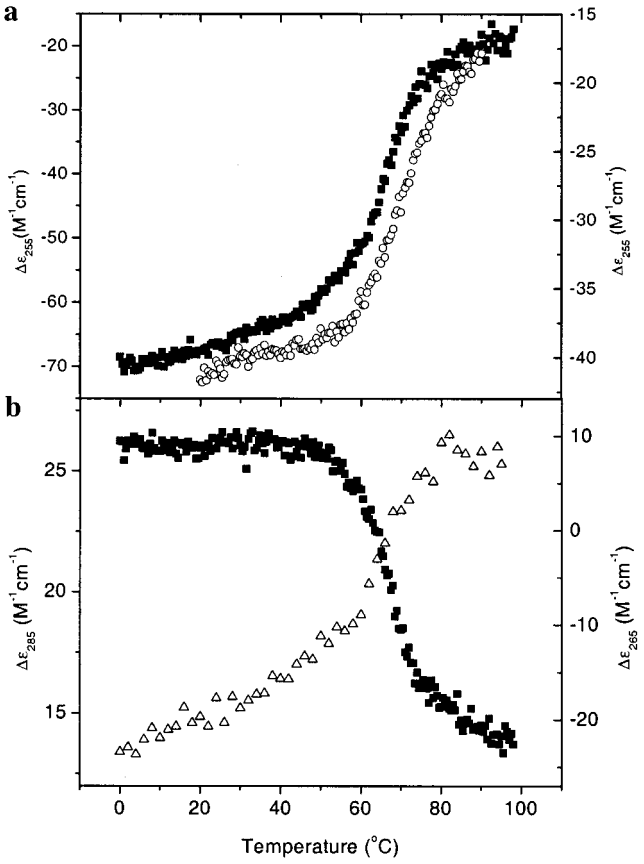

FIGURE 7: Temperature-dependent CD intensities. (a) A_3T_3 (■, left axis) and $(AT)_3$ (○, right axis) duplexes at 255 nm. The concentration of the A_3T_3 duplex was 1.53×10^{-4} M and of the $(AT)_3$ duplex was 1.45×10^{-4} M. (b) Molar ellipticities at 285 (■) and 265 (△) nm of the A_3T_3 duplex as a function of temperature. The A_3T_3 concentration was 1.53×10^{-4} M for the 285 nm data (left axis) and 1.48×10^{-4} M for the 265 nm data (right axis). Sample buffer conditions were as described in the legend of Figure 6.

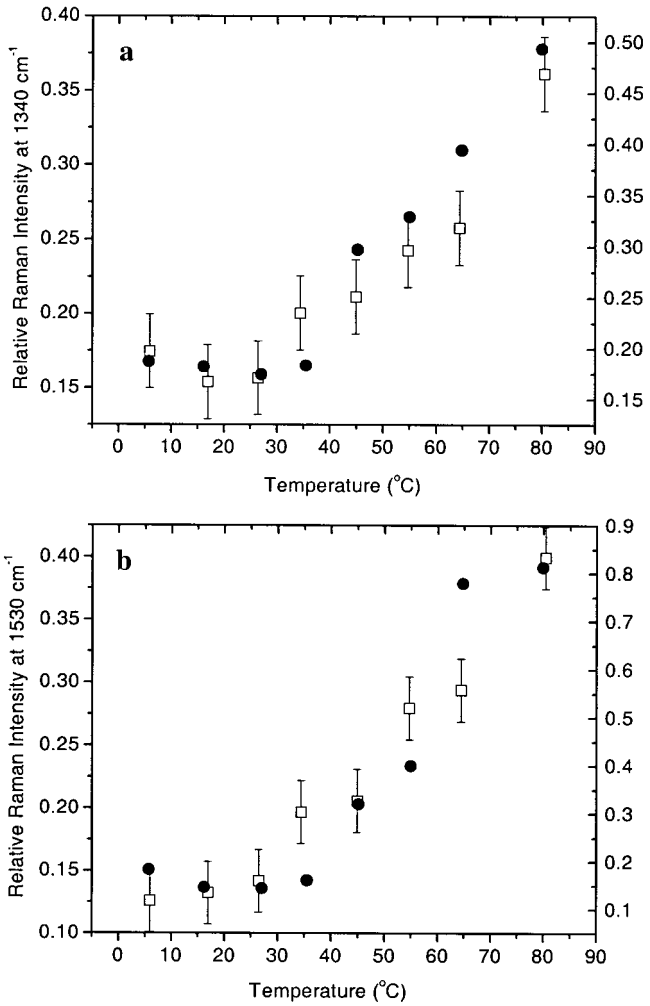

FIGURE 8: Temperature-dependent relative UV Raman intensities of the 1340 and 1530 cm^{-1} modes of the A_3T_3 (□, left axis) and $(AT)_3$ (●, right axis) duplexes obtained with 215 nm excitation. Spectra (not shown) were obtained as a function of temperature and normalized to the intensity standard Na_2SO_4 at 981 cm^{-1}. The DNA concentration was 1.3×10^{-4} M in 10 mM cacodylate buffer (pH 7.0) containing 0.3 M Na_2SO_4. For clarity, error bars are shown for the A_3T_3 data only, and comparable error bars can be drawn for the $(AT)_3$ data.

suggest that the temperature-dependent ellipticity at 285 nm indicates minimal unwinding of the double helix prior to duplex dissociation in the A_3T_3 duplex and is not reflective of the B′- to B-DNA transition.

The 215 nm-Excited UVRR Spectra. UVRR spectra were also acquired using an excitation wavelength of 215 nm, which allows preferential investigation of deoxyribose−phosphate backbone vibrations relative to base vibrations (*20, 21*). These modes are not as strongly enhanced as those observed with 260 nm excitation; nevertheless, temperature-dependent intensity changes can be observed. Figure 8 depicts the temperature-dependent intensity changes for two modes, which are enhanced at this shorter wavelength. The 1340 cm^{-1} mode results from a coupled purine and ribose ring vibration that is conformationally sensitive, occurring at 1343 cm^{-1} in B-form DNA and 1309 cm^{-1} in A-form DNA (*29*). The temperature profile for this mode is

comparable for the two duplexes, indicating that the melting behavior of this mode does not reflect the premelting transition, as observed for other ring stretching modes (Figure 4). Since this vibration contains a ribose-coupled component, we suggest that large conformational changes of the sugar−phosphate backbone are not associated with the premelting transition, which is also indicated by the CD data (see above).

The melting behavior of the cytosine mode at 1530 cm^{-1} was also monitored as a function of temperature (Figure 8b). As for the 1340 cm^{-1} mode, the two duplexes exhibit a similar melting profile for the 1530 cm^{-1} mode. At this frequency, there is minimal contribution from the other bases; thus, the melting profile of this mode reflects that of the cytosine bases only. The profiles are cooperative in shape as expected for standard B-form duplex DNA. The similarity of the A_3T_3 and $(AT)_3$ duplex melting profiles suggests that the premelting transition, which is predominantly observed with 260 nm excitation (Figures 4 and 5), does not extend to the dC and dG residues. The melting profiles obtained with 215 nm excitation strongly suggest that the premelting transition is localized to the base stacking and H-bonding interactions of the dA and dT bases and does not lead to a significant perturbation of the backbone and other bases.

DISCUSSION

The Premelting Transition Is Localized to A·T Base Pairs in A Tracts. Previously, a premelting transition was observed with molecules containing longer A tracts (*12*−*15*, *30*) and was mainly associated with the conversion of B′- to B-DNA (*1*, *11*). The midpoint of this transition occurs at ∼35 °C, as determined by CD and differential scanning calorimetry measurements (Table 2) (*12*, *14*). In this study, UVRR spectra obtained at 260 nm (Figures 4 and 5) provide strong evidence for a premelting transition associated with the A_3T_3 duplex and not the $(AT)_3$ duplex. At this excitation wavelength, base stacking and H-bonding interactions of dA and dT residues are mainly investigated, suggesting that the premelting transition is localized to this region of the DNA duplex. In the premelting temperature range, an increase in molar ellipticity is observed for the A_3T_3 duplex at 255 and 265 nm (Figure 7). Since CD intensities at these wavelengths mainly reflect base stacking interactions (*28*), these results also indicate that the premelting transition is localized to the bases and not the backbone and further support the association of this transition with the A_3T_3 duplex.

Interestingly, UVRR experiments performed with an excitation wavelength of 215 nm suggest that the backbone is minimally involved in the conformational changes associated with the premelting transition. At this excitation wavelength, many base-coupled ribose vibrations are enhanced and the thermal profiles do not show any appreciable differences between the two duplexes (Figure 8). Ellipticity measurements performed at 285 nm show no evidence of untwisting or unwinding of the deoxyribose−phosphate backbone during the premelting transition, in agreement with UVRR results.

It had been previously suggested that changes in the hydration of the minor groove could play an important role in the transition from B′- to B-DNA. Ion binding in the minor groove has also been suggested to play a role in A tract bending (*31*−*33*). Shorter excitation wavelengths (≤220 nm), which enhance the C2═O stretching vibration of thymine residues (*21*), should preferentially monitor H-bonding and ion binding at these sites. UVRR spectra recorded at 220, 215, and 210 nm (data not shown) do not show any evidence of large frequency changes of the dT C2═O vibrations and are not supportive of a large influence from ion binding or hydration of the minor groove in the premelting transition. However, these vibrations are weakly enhanced even at these shorter excitation wavelengths, and minor frequency changes could go undetected. Recent molecular dynamics simulations and X-ray crystallographic results indicate that ion occupancy at these sites is low (*34*−*36*), and with such small occupancies, the associated differences may be difficult to detect in the current UVRR data.

Previous Raman experiments have suggested that poly(dA-dT)·poly(dA-dT) undergoes a premelting transition at temperatures comparable to those of poly(dA)·poly(dT) (*37*). In the study presented here, in which the base composition and length of the DNA duplexes are kept the same albeit with altered base sequences, some evidence for a small premelting transition can be observed in the $(AT)_3$ duplex data (Figure 4). This duplex is expected to exhibit energetic properties similar to those of the poly(dA-dT) heteropolymer. In an X-ray crystal structure determination of several A-T and A-I sequences, pronounced propeller twisting of the adenosine and inosine residues was observed (*8*). Because of the relative proximity of the dA NH_2 groups induced by the propeller twisting, formation of cross-strand bifurcated H-bonds was postulated; therefore, it is possible that similar premelting conformational changes could be observed for A-T sequences. In our study, however, the magnitudes of intensity and frequency changes observed for the $(AT)_3$ duplex are considerably smaller than those observed for the A_3T_3 duplex. For example, the 1335 cm^{-1} mode which arises from stretching vibrations of the dA imidazole ring exhibits a Raman hyperchromicity change of 18% for the A_3T_3 duplex and only 6% for the $(AT)_3$ duplex at 35 °C. Comparable hyperchromicity changes are observed for other dA and dT vibrational modes in the 260 nm-excited UVRR spectra. If the premelting transition primarily results from a change in the degree of propeller twisting and the strength of cross-strand three-centered H-bonds, then these results indicate that the $(AT)_3$ premelting transition is a relatively small perturbation of DNA structure compared to the A_3T_3 premelting transition.

Strength of the Three-Centered H-Bond in the A Tract. The thymidine mode observed at 1650 cm^{-1} arises from coupled stretching vibrations of the C4═O and C5═C6 bonds, with small contributions from N1−H and N3−H bending motions (*23*). Despite the relative complexity of this stretching vibration, a substantial portion of the motion is localized to the C4═O group and is therefore reflective of any perturbations at that site (*21*, *24*). The 10 cm^{-1} frequency upshift observed for the A_3T_3 duplex during the duplex to single-strand transition can be correlated with a decrease in H-bonding strength. In contrast, the UVRR spectra of the $(AT)_3$ duplex exhibit a frequency shift of only 6 cm^{-1} over the same temperature range. The larger frequency shift observed for the A_3T_3 duplex is consistent with the formation of a three-centered H-bond, and the strength of this H-bond can be estimated from the difference in the magnitude of

the frequency shift associated with the global melting of both duplexes.

We estimate the strength of the three-centered H-bond on the basis of the assumption that a linear relationship exists between bond energy and frequency shift, which is valid if the frequency shift is small relative to the overall bond energy (*38*, *39*). The energy of the C═O bond is approximately 743 kJ/mol (*40*); therefore, the change in ΔH of the bond energy can be calculated as

$$\Delta\Delta H = (10/1655) \times 743 \text{ kJ/mol} = 4.5 \text{ kJ/mol}$$

A similar calculation for the $(AT)_3$ duplex yields a value of 2.6 kJ/mol. A comparison of these bond energies suggests that the strength of the three-centered H-bond in the A_3T_3 duplex is 1.9 kJ/mol, or 0.46 kcal/mol. In the X-ray crystal structure of this sequence, only one three-centered H-bond was observed from the central A5 residue to the T20 and T19 residues (Figure 1). UVRR spectroscopy examines all the dA and dT residues in the A tract, and the observed frequency shift represents an average for all the dT residues present. Thus, the observed frequency shift for the three-centered H-bond could be larger than what is observed, causing the calculated bond enthalpy to represent a lower limit. In fact, UVRR difference spectra obtained between the A_3T_3 and $(AT)_3$ duplexes at low temperatures are strongly suggestive of a larger frequency shift (*18*). A recent study of the interaction between 4′,6-diamidine-2-phenylindole and DNA estimated that each bifurcated H-bond contributed approximately 2 kcal/mol in binding energy (*41*). This finding is consistent with the possibility that our determined bond enthalpy represents a lower limit for the three-centered H-bond.

The determined enthalpy of the three-centered H-bond is considerably weaker (∼0.5 kcal/mol) than the bond energies typically reported for Watson−Crick hydrogen bonds (2−3 kcal/mol) (*3*). However, the relative frequency shifts (4 vs 6 cm^{-1}) would suggest that the strength of the three-centered H-bond is approximately 75% of that of the dT C4═O··· dA NH_2 Watson−Crick H-bond. Both bond enthalpies are probably underestimated because the mode is not 100% localized to the dT C4═O stretch. If the van't Hoff enthalpy for the premelting transition is considered, then it appears that the three-centered H-bond is one of several factors contributing to the stabilization of B′-DNA. The CD data can be analyzed using the model of Marky and Breslauer (*42*, *43*), assuming independent premelting and duplex transitions. This analysis yields a van't Hoff enthalpy of 15.1 ± 3.3 kcal/mol with a T_m of 30 °C for the premelting transition. These values are consistent with those previously reported for poly(dA)·poly(dT) (*13*, *30*) and for $d(GA_4T_4C)_2$ (*12*) (Table 2). In terms of the total number of base pairs, a value of 1.3 kcal/mol per bp is obtained, which suggests that the three-centered H-bond potentially contributes approximately 35% of the stabilization of the A5−T20 base pairs in the B′ conformation or the premelted state. The ΔH associated with the premelting transition is often reported in terms of the cooperative unit, which has been estimated to be 11 bp (*11*). The current work indicates that conformational changes associated with the premelting transition are primarily confined to A·T base pairs, but provide no information regarding the length of the cooperative unit. Molecular dynamics (*35*), NMR (*10*), and X-ray crystal structure (*44*) studies of A tract-containing sequences have indicated that the observed bending is a consequence of A tract and non-A tract regions of the sequence. Consequently, the length of the cooperative unit for the A_3T_3 duplex is not defined, and we prefer to consider the energetics of premelting and the three-centered H-bond in terms of the number of A·T base pairs and A-A base steps (Table 2).

If the strength of the three-centered H-bond is considered in terms of the total number of A·T base pairs or A-A base steps, then the overall contribution to A tract stabilization ranges from 10 to 20% (Table 2). This partial stabilization from three-centered H-bonds is supported by a recent molecular dynamics simulation of three dodecamer A tract sequences, which indicated that the three-centered H-bonds are a consequence of rather than a driving force for forming the highly propeller-twisted conformation (*45*). Other sources of stabilization potentially arise from improved base stacking interactions (*4*, *45*) and ion binding in the minor groove (*31*, *33*, *46*).

In summary, these experiments reveal that the three-centered H-bond does exist in the premelting state of the A_3T_3 duplex and has an estimated strength of ∼0.5 kcal/mol. UVRR spectroscopic evidence for the presence of the three-centered H-bond was previously observed in the homopolymer poly(dA)·poly(dT) (*15*); however, the frequency shifts are not directly comparable because dipole−dipole coupling of adjacent dT C4═O groups in the homopolymer leads to splitting of the C4═O mode. Nevertheless, the current and previous data (*15*) indicate that the three-centered H-bond is present in relatively short and long A_n tracts and is a structural characteristic of A tract DNA. The role of this H-bond in the cooperativity associated with A tract-induced bending (*17*) needs to be evaluated with additional experiments on phased A tracts. In the current study, the strength of the three-centered H-bond is directly determined using UVRR spectroscopy and compared to $\Delta H_{premelt}$. This comparison reveals that the three-centered H-bond is responsible for a portion but not all of the stabilization associated with the propeller-twisted dA residues in A_n tracts. In addition, the 260 nm- and 215 nm-excited resonance Raman data indicate that the conformational changes associated with the premelting transition are primarily confined to the dA and dT bases of the A_nT_n tract. The spectroscopic changes observed for this transition mainly result from a reduction in the extent of base stacking interactions and H-bonding strength of the dA and dT residues.

ACKNOWLEDGMENT

A.P.W. thanks Ken Breslauer (Rutgers University) for the generous use of his research facilities.

SUPPORTING INFORMATION AVAILABLE

Figures showing UV absorbance melts at 260 nm and UVRR spectra obtained with 215 nm excitation of the A_3T_3 and $(AT)_3$ duplexes. This material is available free of charge via the Internet at http://pubs.acs.org.

REFERENCES

1. Crothers, D. M., and Shakked, Z. (1999) in *Oxford Handbook of Nucleic Acid Structure* (Neidle, S., Ed.) pp 455−470, Oxford University Press, Oxford, U.K.

2. Hagerman, P. J. (1990) *Annu. Rev. Biochem. 59*, 755−781.
3. Sinden, R. R. (1994) *DNA Structure and Function*, Academic Press, San Diego.
4. Nelson, H. C. M., Finch, J. T., Luisi, B. F., and Klug, A. (1987) *Nature 330*, 221−226.
5. Yoon, C., Prive, G. G., Goodsell, D. S., and Dickerson, R. E. (1988) *Proc. Natl. Acad. Sci. U.S.A. 85*, 6332−6336.
6. Edwards, K. J., Brown, D. G., Spink, N., Skelly, J. V., and Neidle, S. (1992) *J. Mol. Biol. 226*, 1161−1173.
7. Dickerson, R. E., Goodsell, D., and Kopka, M. L. (1996) *J. Mol. Biol. 256*, 108−125.
8. Shatzky-Schwartz, M., Arbuckle, N. D., Eisenstein, M., Rabinovich, D., Bareket-Samish, A., Haran, T. E., Luisi, B. F., and Shakked, Z. (1997) *J. Mol. Biol. 267*, 595−623.
9. Michalczyk, R., and Russu, I. M. (1998) in *Structure, Motion, Interaction and Expression of Biological Macromolecules, Proceedings of the Tenth Conversation* (Sarma, R. H., and Sarma, M. H., Eds.) pp 181−189, Adenine Press, Albany, NY.
10. MacDonald, D., Herbert, K., Zhang, X., Pologruto, T., and Lu, P. (2001) *J. Mol. Biol. 306*, 1081−1098.
11. Breslauer, K. J. (1991) *Curr. Opin. Struct. Biol. 1*, 416−422.
12. Park, Y.-W., and Breslauer, K. J. (1991) *Proc. Natl. Acad. Sci. U.S.A. 88*, 1551−1555.
13. Chan, S. S., Breslauer, K. J., Hogan, M. E., Kessler, D. J., Austin, R. H., Ojemann, J., Passner, J. M., and Wiles, N. C. (1990) *Biochemistry 29*, 6161−6171.
14. Chan, S. S., Breslauer, K. J., Austin, R. H., and Hogan, M. E. (1993) *Biochemistry 32*, 11776−11784.
15. Chan, S. S., Austin, R. H., Mukerji, I., and Spiro, T. G. (1997) *Biophys. J. 72*, 1512−1520.
16. Tabernero, L., Verdaguer, N., Coll, M., Fita, I., van der Marel, G., van Boom, J. H., Rich, A., and Aymami, J. (1993) *Biochemistry 32*, 8403−8410.
17. Haran, T. E., and Crothers, D. M. (1989) *Biochemistry 28*, 2763−2767.
18. Sokolov, L., Wojtuszewski, K., Tsukroff, E., and Mukerji, I. (2000) *J. Biomol. Struct. Dyn. Conversation 11*, 327−334.
19. Wojtuszewski, K., Hawkins, M. E., Cole, J. L., and Mukerji, I. (2001) *Biochemistry 40*, 2588−2598.
20. Mukerji, I., Sokolov, L., and Mihailescu, M.-R. (1998) *Biopolymers 46*, 475−487.
21. Fodor, S. P. A., Rava, R. P., Hays, T. R., and Spiro, T. G. (1985) *J. Am. Chem. Soc. 107*, 1520−1529.
22. Toyama, A., Hanada, N., Abe, Y., Takeuchi, H., and Harada, I. (1994) *J. Raman Spectrosc. 25*, 623−630.
23. Aida, M., Kaneko, M., Dupuis, M., Ueda, T., Ushizawa, K., Ito, G., Kumakura, A., and Tsuboi, M. (1997) *Spectrochim. Acta A53*, 393−407.
24. Toyama, A., Takeuchi, H., and Harada, I. (1991) *J. Mol. Struct. 242*, 87−98.
25. Tunis-Schneider, M. J. B., and Maestre, M. F. (1970) *J. Mol. Biol. 52*, 521−541.
26. Vorlícková, M., Johnson, W. C., Jr., and Kypr, J. (1994) *Biopolymers 34*, 299−301.
27. Santa-Lucia, J., Jr., Allawi, H. T., and Seneviratne, P. A. (1996) *Biochemistry 35*, 3555−3562.
28. Baase, W. A., and Johnson, W. C., Jr. (1979) *Nucleic Acids Res. 6*, 797−814.
29. Toyama, A., Takino, Y., Takeuchi, H., and Harada, I. (1993) *J. Am. Chem. Soc. 115*, 11092−11098.
30. Herrera, J. E., and Chaires, J. B. (1989) *Biochemistry 28*, 1993−2000.
31. Hud, N. V., and Feigon, J. (1997) *J. Am. Chem. Soc. 119*, 5756−5757.
32. Hud, N. V., Sklenar, V., and Feigon, J. (1999) *J. Mol. Biol. 286*, 651−660.
33. McFail-Isom, L., Sines, C. C., and Williams, L. D. (1999) *Curr. Opin. Struct. Biol. 9*, 298−304.
34. McConnell, K. J., and Beveridge, D. L. (2000) *J. Mol. Biol. 304*, 803−820.
35. McConnell, K. J., and Beveridge, D. L. (2001) *J. Mol. Biol.* (in press).
36. Strahs, D., and Schlick, T. (2000) *J. Mol. Biol. 301*, 642−663.
37. Movileanu, L., Benevides, J. M., and Thomas, G. J., Jr. (1999) *J. Raman Spectrosc. 30*, 637−649.
38. Badger, R. M., and Bauer, S. H. (1937) *J. Chem. Phys. 5*, 839−851.
39. Thorogood, H., Waters, T. R., Parker, A. W., Wharton, C. W., and Connolly, B. A. (1996) *Biochemistry 35*, 8723−8733.
40. Pauling, L. (1960) *The Nature of the Chemical Bond*, 3rd ed., Cornell University Press, Ithaca, NY.
41. Lan, T., and McLaughlin, L. W. (2001) *J. Am. Chem. Soc. 123*, 2064−2065.
42. Marky, L. A., and Breslauer, K. J. (1987) *Biopolymers 26*, 1601−1620.
43. Breslauer, K. J. (1995) *Methods Enzymol. 259*, 221−242.
44. Hizver, J., Rozenberg, H., Frolow, F., Rabinovich, D., and Shakked, Z. (2001) *Proc. Natl. Acad. Sci. U.S.A. 98*, 8490−8495.
45. Sherer, E. C., Harris, S. A., Soliva, R., Orozco, M., and Laughton, C. A. (1999) *J. Am. Chem. Soc. 121*, 5981−5991.
46. Young, M. A., Jayaram, B., and Beveridge, D. L. (1997) *J. Am. Chem. Soc. 119*, 59−69.

BI010918I